

Measurements of Spin Structure Function $G_1(P)$ and $G_1(D)$ for Proton and Deuteron at SLAC E143*

Tingjun Liu

Stanford Linear Accelerator Center
Stanford University
Stanford, CA 94309

SLAC-Report-696
January 1996

Prepared for the Department of Energy
under contract number DE-AC03-76SF00515

Printed in the United States of America. Available from the National Technical Information Service, U.S. Department of Commerce, 5285 Port Royal Road, Springfield, VA 22161.

* Ph.D. thesis, University of Virginia, Charlottesville, VA, 22901

MEASUREMENTS OF SPIN STRUCTURE FUNCTION
 g_1^p AND g_1^d FOR
PROTON AND DEUTERON AT SLAC E143

Tingjun Liu
Jiangxi, China

B.S., Beijing University, 1989
M.S., University of Virginia, 1993

A Dissertation Presented to the Graduate
Faculty of the University of Virginia
in Candidacy for the Degree of
Doctor of Philosophy

Department of Physics

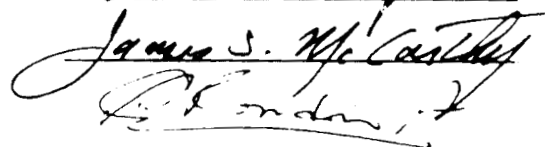
University of Virginia

January 1996



Robert G. Bryant

Donal B. Day



James S. McCarley

Abstract

E143 [1] [2] was a high precision measurement of the proton and deuteron spin structure functions g_1 and g_2 in SLAC's End Station A facility, with longitudinally and transversely polarized NH₃ and ND₃ targets, and a longitudinally polarized electron beam. The experiment was done at beam energies of 29, 16 and 9.7 GeV. The deeply inelastic scattered electrons were detected by two independent spectrometers at 4.5° and 7° relative to the incident electron beam. At a beam energy of 29 GeV, the measurements covered the Bjorken x range from 0.03 to 0.8, and the Q^2 range from 1.2 (GeV/c)² to 9.8 (GeV/c)². It was found that the $\int_0^1 g_1^p(x, Q^2) dx$ is more than two standard deviations away from the Ellis-Jaffe sum rule, and the corresponding deuteron integral is more than three standard deviations away from the Ellis-Jaffe's rule, but the Bjorken sum rule is consistent with the experimental data. Tests of the sum rules at different values of Q^2 , and the implications of these results for the quark-parton model have also been done.

Acknowledgments

First and foremost, I am extremely grateful, to my research advisor James McCarthy, for all of his help and guidance throughout my research. Especially, I am thankful for his care for my professional growth. With deep appreciation, I also would like to thank Donald Crabb, Donal Day, Ralph Minehart, Xiaotong Song, and other members of the polarized target group, for their help and support.

This experiment was a joint effort of over eighty physicists and students at SLAC. It has been a wonderful learning experience for me, to be in this experiment. It has been a great pleasure working with Todd Averett, a fellow University of Virginia student, as well as the other seven graduate students on this experiment: Johannes Bauer, Robin Erbacher, Jeff Fellbaum, Philippe Grenier, Masao Kuriki, Paul Raines and Philipp Steiner, during data-taking and subsequent analysis.

During my stay at the University of Virginia, I am fortunate to have known many great people. In particular, my two "American mothers": Mrs. Gerda Pirsch and Mrs. Marian Limber. As my family hosts, they have given me much love and care. I have also enjoyed the friendship of Jim Shea and Thian-Teck Ong, as well as their wisdom and sense of humor.

My very special thanks are due to Oscar Rondon-Aramayo, co-spokesperson of this experiment. He has given me an enormous amount of help and guidance over the years, without which this work would not have been possible. He has given me so many inspiring ideas and much-needed confidence. All of his efforts will surely help me throughout my career.

To my parents and family,
for their love, and confidence,
in everything I do.

Contents

Table of Contents	4
List of Figures	8
List of Tables	11
1 INTRODUCTION	14
1.1 Overview	14
1.2 Constituent quark model	16
1.3 Spin Crisis	19
1.4 Formalism	20
1.5 Virtual Photon-Nucleon Asymmetry	24
1.6 Bjorken Sum Rule	27
1.7 Goals of E143	29
2 APPARATUS	30
2.1 Polarized Electron Source	31
2.2 A-bend	34
2.3 Electron Polarization and Spin Precession	36
2.4 Beam Steering And Monitoring Device	37
2.4.1 Beam rastering	37

2.4.2	Foil arrays	39
2.4.3	Good and bad spill counters	39
2.4.4	Toroid charge monitor	40
2.5	Møller Polarimetry	40
2.6	Spectrometer Systems	46
2.7	Electronics	53
2.8	Polarized target	57
2.8.1	Overview	57
2.8.2	Operation principles	57
2.8.3	Target setup	61
2.8.4	Polarization measurements and performance	64
2.8.5	Other polarization measurements	70
2.8.6	Target materials	73
2.8.7	A hypothesis on the frequency modulation to improve deuteron polarization	74
3	DATA ANALYSIS AND RESULTS	79
3.1	Extraction of Raw Electron Counts	79
3.1.1	Exclusion of the Bad Runs	79
3.1.2	Finding electron rates	80
3.2	Longitudinal and Transverse Asymmetries A^{\parallel} and A^{\perp}	85
3.2.1	Beam heating Corrections	86
3.2.2	A model to calculate the target depolarization in beam	91
3.2.3	Target Temperature Variation in Beam	95
3.2.4	Depolarization Calculation	99
3.2.5	Dead time corrections	108

3.2.6	Dilution factor and nitrogen corrections	114
3.2.7	Averaging the asymmetries over all the runs and calculating statistical errors	118
3.2.8	Corrections for positron and pion contamination	120
3.2.9	Radiative Corrections	122
3.2.10	Effects on statistical error	127
3.3	g_1 and Its Integral	128
3.3.1	g_1 at the measured Q^2 and evolved to $Q_0^2 = 3\text{GeV}^2$	128
3.3.2	g_1 integral	135
3.3.3	Extraction of neutron information and B-J sum	136
3.4	Γ_1^p and Γ_1^d from different electron definitions	138
3.4.1	An alternative assumption in Q^2 evolution	138
3.5	Results of the Systematic Errors	140
4	Conclusion	141
4.1	Results of Various E143 Sums	141
4.2	Quark Helicity Contents	142
4.2.1	Constituent quark model review	142
4.2.2	Conventional method for E143	144
4.2.3	Discussions on F and D	146
4.2.4	An alternative method for E143	146
4.3	Comparisons with Other experiments	148
4.4	Comparison with a Model	150
4.5	Summaries	151
A	Systematic Errors	163
A.1	Algorithm	163

CONTENTS

7

A.2 Calculations of the error 161

B Improvements in this Analysis 174

List of Figures

1.1	Variables in deep inelastic electron-nucleon scattering	20
2.1	SLAC polarized electron source	31
2.2	Energy bands in GaAs	32
2.3	Energy bands in strained GaAs compared to unstrained case.	33
2.4	a.) Quantum efficiency (QE) of the SLAC polarized electron source cathode during E143. b.) The measured and fitted beam polarization versus the cathode quantum efficiency during E143.	35
2.5	E143 raster pattern at the foil arrays. The magnification at the target face to the foil arrays is 0.866	38
2.6	E143 Møller polarimetry setup	43
2.7	Spatial distribution of the Møller scattered electrons at the mask (top), magnet exit (middle) and the momentum slit downstream (bottom)	44
2.8	E143 spectrometers centered at scattering angles of 4.5° and 7°	47
2.9	Trajectories of electrons with different momenta and scattering angles in SP7, drawn relative to the central ray of 12.5 GeV and nominal scattering angle.	49
2.10	Electron and proton Zeeman effect in a 5 Tesla field.	58
2.11	Deuteron Zeeman effect in a 5 Tesla field.	60
2.12	E143 polarized target.	62

LIST OF FIGURES

2.13	Target inserts used in E143.	63
2.14	Typical proton TE signal	66
2.15	Typical deuteron TE signal	67
2.16	Typical proton enhanced signal	68
2.17	Typical deuteron enhanced signal	68
2.18	Spread of the proton TE calibration constant measured at different time.	70
2.19	^{15}N polarization versus ND_3 polarization.	71
2.20	^{15}N polarization versus NH_3 polarization.	72
2.21	NH_3 polarization vs. total charge (in units of 10^{14} electrons.)	73
2.22	Improved ND_3 polarization with frequency modulation.	75
2.23	Four transitions relevant to ND_3 polarization	76
3.1	Two polarization regions with rastering	88
3.2	Single ammonia bead model in beam	93
3.3	NH_3 saturation polarization vs. temperature	94
3.4	NH_3 bead temperature variation in beam	100
3.5	NH_3 bead depolarization	102
3.6	Early stage of NH_3 bead polarization drop after beam turned on.	103
3.7	NH_3 bead polarization variation	104
3.8	NH_3 bead polarization oscillation in C.W. beam, with rastering frequency of 10 Hz.	107
3.9	The α^3 -order Feymann diagrams for deep inelastic lepton nucleon scattering	124
3.10	Proton g_1 value at $Q^2=3 \text{ GeV}^2$ assuming A_1 and A_2 to be Q^2 independent. Combined from both spectrometers.	133
3.11	Deuteron g_1 value at $Q^2=3 \text{ GeV}^2$ assuming A_1 and A_2 to be Q^2 independent. Combined from both spectrometers.	134

3.12	I_1^p for electron definitions 6 through 28	139
4.1	A_1^p from E143 and SMC	149
4.2	A_1^d from E143 and SMC	149
4.3	g_1^n from E143 and E142	150
4.4	Comparison of E143 g_1^p with a model	151
4.5	A_1^p vs. x	153
4.6	A_1^d vs. x	160
4.7	g_1^p vs. x	161
4.8	A_1^n vs. x	162

List of Tables

1.1	Quark classifications	16
2.1	Hodoscope plane specifications for SP4. Width, length and thickness are in units of mm.	51
2.2	Hodoscope plane specifications for SP7. Width, length and thickness are in units of mm.	52
2.3	Typical prescalar factors	54
2.4	Optimal polarizing frequency for maximum polarization.	75
3.1	Vertical foil array corrections	81
3.2	Different electron definitions, where definition 6 through 29 are used to study target settling.	83
3.3	Beam heating results	89
3.4	Beam heating results	90
3.5	Comparison of the predicted rates, from Poisson distribution ("prate"), and from the modified version of it ("orate")	112
3.6	Various trigger frequency distributions ("tfreq") for run 2558 and SP7.	113
3.7	Table for g_1^p	131
3.8	Table for g_1^d	132

3.9	Results of $\int g_1^p$, $\int g_1^d$ and the B-J sum. All the errors except from the low x region are statistical only.	137
3.10	Results of $\int g_1^p$ and $\int g_1^d$ for different electron definitions. Statistical errors only.	138
3.11	Comparisons of various sums between different Q^2 independent assumptions.	139
3.12	Systematic errors in Γ_1^p , Γ_1^d , Γ_1^{p-n} and Γ_1^n	140
4.1	Summary of quark helicity components	145
4.2	Quark helicity components from an alternative method	147
4.3	Comparison of E143, SMC, E142 and theoretical results, where SMC Γ_1^p and Γ_1^{p-n} are evaluated at $Q^2=5 \text{ GeV}^2$, and E142 Γ_1^n is evaluated at $Q^2=2 \text{ GeV}^2$	148
4.4	Spectrometer 4 results for NH_3	151
4.5	Spectrometer 7 results for NH_3	155
4.6	Spectrometer 4 results for ND_3	156
4.7	Spectrometer 7 results for ND_3	157
4.8	A_1^p and A_1^d after combining the two spectrometers.	158
4.9	Extracted g_1^n and A_1^n	159
A.1	Errors in g_1 sums due to various uncertainties associated with dilution factor.	166
A.2	Systematic errors on g_1^p	170
A.3	More systematic errors on g_1^p	171
A.4	Systematic errors on g_1^p	172
A.5	More systematic errors on g_1^d	173

B.1 $\int g_1^p$ and $\int g_1^d$ results, from this analysis and published values for E143,
using g_1/F_1 or A_1 and A_2 to be Q^2 independent assumptions. 178

B.2 $\int g_1^p$ and $\int g_1^d$ results at different phases of this analysis 178